Desalination and Water Treatment
www.deswater.com
doi: 10.5004/dwt.2023.29874

309 (2023) 185–192
October

Performance of an internally fan circulated air gap membrane distillation (AGMD) unit

Dahiru U. Lawal[a,*], Ibrahim B. Mansir[b,f], Binash Imteyaz[c], Abba Abdulhamid Abubakar[d], Mansur Aliyu[e], Suhaib M. Alawad[c]

[a]*Interdisciplinary Research Center for Membranes and Water Security, KFUPM, Saudi Arabia, email: dahiru.lawal@kfupm.edu.sa*
[b]*Department of Mechanical Engineering, Prince Sattam bin Abdulaziz University, Saudi Arabia*
[c]*Interdisciplinary Research Center for Renewable Energy and Power Systems, KFUPM, Saudi Arabia*
[d]*Mechanical Engineering Department, Interdisciplinary Research Center for Advanced Materials, KFUPM, Saudi Arabia*
[e]*Interdisciplinary Research Center for Hydrogen and Energy Storage, KFUPM, Saudi Arabia*
[f]*Department of Mechanical Engineering, College of Engineering in Al-Kharj, Prince Sattam bin Abdulaziz University, Al-Kharj, 11942, Saudi Arabia*

Received 30 June 2023; Accepted 23 August 2023

ABSTRACT

This work involves an experimental investigation of a novel air gap membrane distillation (AGMD) unit with an installed circulating fan within the condensation chamber. The installed fan breaks the resistance to mass and heat transfer in the gap chamber by inducing fluid mixing and a turbulent dissipation rate, which enhances the overall mass and heat transfer characteristics of the system and consequently the overall performance of the system. The system performance, such as vapor flux, specific thermal energy consumption (STEC), and desalinated water cost, of the new AGMD is evaluated and compared to the traditional AGMD system. The influence of fan design variables, including fan revolution, fan thickness, and fan diameter, on system performance is investigated. Furthermore, the effect of feed water temperature on the system's performance is assessed and presented. Results indicate that fan speed significantly improves the performance of the new AGMD system compared to conventional AGMD designs. Fan thickness recorded a marginal effect, and fan diameter registered some influence, while fan revolution exhibits the strongest impact on the system's performance. The new system can attain a maximum flux and minimum STEC of 34.16 kg/m^2·h and 710.72 kWh/m^3, respectively, as against the conventional units, which registered a peak vapor flux and lowest STEC of 17.69 kg/m^2·h and 1,141.25 kWh/m^3, respectively.

Keywords: Experimental study; Membrane distillation (MD); Water desalination; Novel air gap membrane distillation design; Productivity; Cost; Energy analysis

1. Introduction

Freshwater production from water resources such as seawater and brackish water through desalination has been on the increase due to the growing pressure emanating from rising population, agricultural, and industrial demands. Over the years, several desalination techniques have evolved, some of which have been industrialized and reached maturity, while others are still in the small-scale and developmental stages. Among the matured and developed desalination processes are reverse osmosis, multi-stage flash, and multi-effect distillation. The developing and emerging desalination technologies, including forward osmosis, humidification dehumidification, membrane distillation, electrodialysis, capacitive deionization, freeze desalination, and electrodialysis reversal, are growing and drawing the attention of many investigators, researchers, innovators, investors, and stockholders due to their potential to provide sustainable and affordable freshwater to meet human needs. In particular, membrane distillation (MD) systems

* Corresponding author.

Presented at the European Desalination Society Conference on Desalination for the Environment: Clean Water and Energy, Limassol, Cyprus, 22–26 May 2023

offer many benefits, including high salt rejection, low-cost components, low operating pressure, the ability to handle high feed salinity, simplicity in module design, easy module installation, and demand no technical experts in their operation and maintenance. MD processes require temperatures below boiling points and therefore can be driven by renewable energy (e.g., solar energy) and low-grade waste heat. Furthermore, the MD system can also be integrated with other systems for effective improvement in the overall performance of the hybrid system. These make the MD technology desirable and favorite for remote settings, small-scale, and decentralized freshwater production technology. The MD process applied a thermal gradient as a driving force for vapor permeation across the membrane pores.

Over the years, several attempts have been made to improve the performance of MD systems through enhanced membrane [1–9], module modification [10–19], process improvement [20–29], multi-stage and multi-effect [30–33], and hybridization with other systems [30,31,34–41]. The aforementioned studies are all in an attempt to take the MD technology into industrial full-scale implementation, which is yet to be achieved due to its low permeate flux and high energy requirements. Among the MD performance improvement strategies, MD module improvement has a lot of potential. To this end, an air-gap membrane distillation (AGMD) module with a single coolant chamber and double feed chambers has been proposed [42]. The study concluded that the module cost and module footprint were reduced with the new design. A water-gap membrane distillation (WGMD) system with an external gap recirculating line has also been proposed and investigated [43]. The external gap stream circulation was reported to have enhanced the system flux significantly by 80%–96% and the system gained output ratio by about 5%–22%. To address the problem of gap flooding in AGMD, porous wick conductive condensers have been adopted to fill the gap chamber of AGMD [17]. Results indicated that the used porous condensers enhanced the system productivity, GOR, and energy efficiency by about 144%, 98%, and 40%, respectively. A conductive gap membrane distillation where a conductive spacer was installed in the gap chamber of AGMD has been presented [44]. It was found that a conductive gap doubles the GOR of the system when compared to a WGMD and is 2.4-folds higher than the GOR of an AGMD. A material gap MD has also been proposed and examined by Francis et al. [45], where different materials such as de-ionized water, sand, polypropylene, and polyurethane mesh were employed to fill the gap of an AGMD cell. Results indicated improved performance for the material gap, in which the system flux is enhanced between 200%–800% over the regular AGMD module. An AGMD module with a non-porous finned copper tube condenser was investigated and attained a flux that is 2–5 times higher than a regular AGMD module [46]. To increase the condensation surface area in the AGMD module by 45%, a cylindrical copper tube with continuous helical fins over it was used [47]. The presence of helical fins in the gap chamber also decreases the gap thickness by about 64%. A network of stainless-steel multiple cooling channels has also been employed to decrease environmental heat loss and enhance the system thermal efficiency and vapor flux of the AGMD module [48]. The system reached a maximum thermal efficiency and mass flux of 81.7% and 12.5 L/m^2·h, respectively. The study reported a mean of 58% higher thermal efficiency than the hollow-fiber DCMD cell and 22% higher flux than the mean vapor flux of the AGMD cell. Recently, an AGMD module with an installed internal rotating fan inside the gap chamber was proposed and investigated [14]. At a fan revolution of 4,000 rev/min, the new AGMD module recorded about 250%, 77%, and 67% enhancements in vapor flux, specific thermal energy consumption, and gained output ratio, respectively.

The work presented in [14] examined and discussed the effect of system operating variables including feed temperature, feed flowrate, cold stream temperature, cold stream flowrate, feed salinity, air-gap thickness, and fan rotational speed. However, the influence of fan design parameters such as fan diameter and fan thickness, which may affect the overall system performance, is lacking. It is important to examine how the system flux and energy consumption respond to changes in these fan design variables. Therefore, the current study is intended to investigate the impact of fan thickness and fan diameter on system performance. Furthermore, the cost of freshwater from the proposed AGMD system is analyzed. The findings from this work are paramount to understanding fan behavior in the new AGMD system.

2. Materials and experimental apparatus

2.1. Materials

To investigate the influence of fan design variables on the system flux and specific thermal energy consumption, a commercially available flat sheet PTFE membrane purchased from Tisch Scientific was utilized. The membrane has a mean pore size of 0.26 μm, which was measured using a capillary flow porometer (3 Gzh, Quantachrome Instruments, USA), and the membrane pore size distribution is shown in Fig. 1. A gravimetric analysis was adopted to calculate the membrane porosity, while the membrane liquid entry pressure (LEP) was measured using a laboratory-made LEP set-up. The membrane overall thickness, including the active and support layers, was measured using a LITEMATIC VL-50A Mitutoyo precision device, and the membrane hydrophobicity (contact angle) was measured by a DM-501 Kyowa

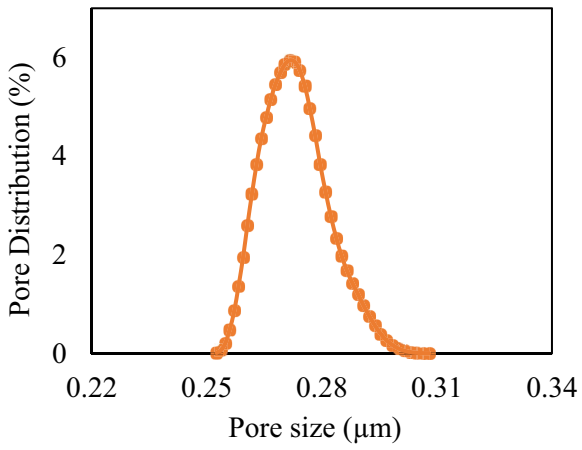

Fig. 1. Pore-size distribution of the used PTFE membrane.

Interface Science Co. Ltd., Japan goniometer. Some of the field emission scanning electron microscope (FE-SEM) images representative of the used membrane are depicted in Fig. 2, and the detailed specification of the used membrane is tabulated in Table 1.

A synthetic seawater of 35 g/L was simulated in the lab by dissolving 350 g of NaCl in 10 L of di-ionized water.

2.2. Experimental test rig

The schematic representation of the lab-scale AGMD set-up is illustrated in Fig. 3. The major components of the setup include a novel AGMD module, a hot water recirculating bath, and a cold water recirculating bath. The AGMD module consists of a feed chamber, a gap chamber, a coolant chamber, a fan blade, and a DC motor. The hot and cold chambers have the same dimensions (90.25 mm × 80 mm × 4.5 mm) each and are made from clear acrylic. A 1.5 mm thick brass plate was used as a condensation surface. The gap chamber has a dimension of 90.25 mm × 80 mm × 11 mm. An aluminum fan blade with a thickness of 0.6 mm and a diameter of 60 mm was installed in the gap chamber. To study the effect of fan thickness on system performance, fan thicknesses of 0.6, 1.0, and 2.0 mm were considered. Furthermore, two different fan diameters of 40 and 60 mm, as shown in Fig. 4, were considered in examining the effect of fan diameter on the system's performance. The fan blade was connected to the DC motor through an aluminum shaft of 5 mm diameter. A 12 V DC motor was used to drive the fan in the gap chamber. A 3-D exploded image showing each component of the new AGMD module and the actual photo of the new AGMD module are presented in Fig. 5.

For the MD bench-scale experiments, the feed saline water is heated in the recirculating hot bath to the desired temperatures (50°C, 60°C, 70°C, and 80°C) and fed to the feed side of the MD module at a rate of 3 L/min, while the coolant stream is chilled to 20°C in the recirculating cold bath and fed at a rate of 3 L/min to the coolant side of the MD module. The fan revolution varied between 500 and 2,000 rpm.

2.3. Analytical methods

The AGMD system's performance is evaluated in terms of water flux (J_w) and specific thermal energy consumption (STEC). The new AGMD flux and salt rejection efficiency (SR) are calculated from Eqs. (1) and (2), respectively.

$$J_W = \frac{W}{t \times A_{\text{em}}} \tag{1}$$

$$\text{SR} = \frac{C_f - C_p}{C_f} \times 100\% \tag{2}$$

Table 1
PTFE membrane properties

Properties		Value
Total thickness		159 ± 18 μm
Pore size	Mean	0.26 μm
	Min.	0.27 μm
	Max.	0.29 μm
Porosity		68.10%
Water contact angle		112.2°
Liquid entry pressure		2.9 ± 0.3 bar
Effective area		3.081×10^{-3} m^2

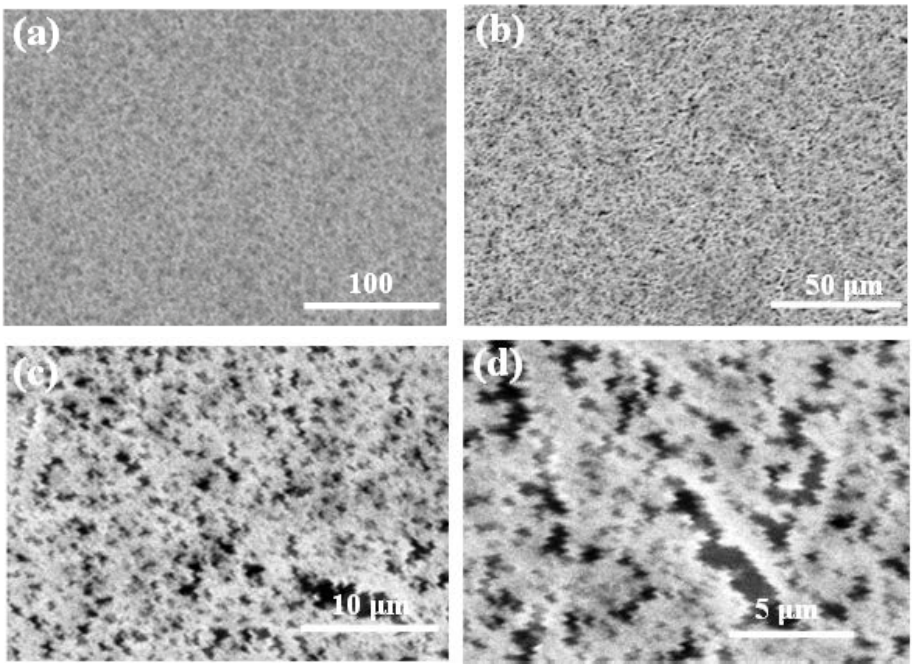

Fig. 2. SEM images of the used commercial PTFE membrane.

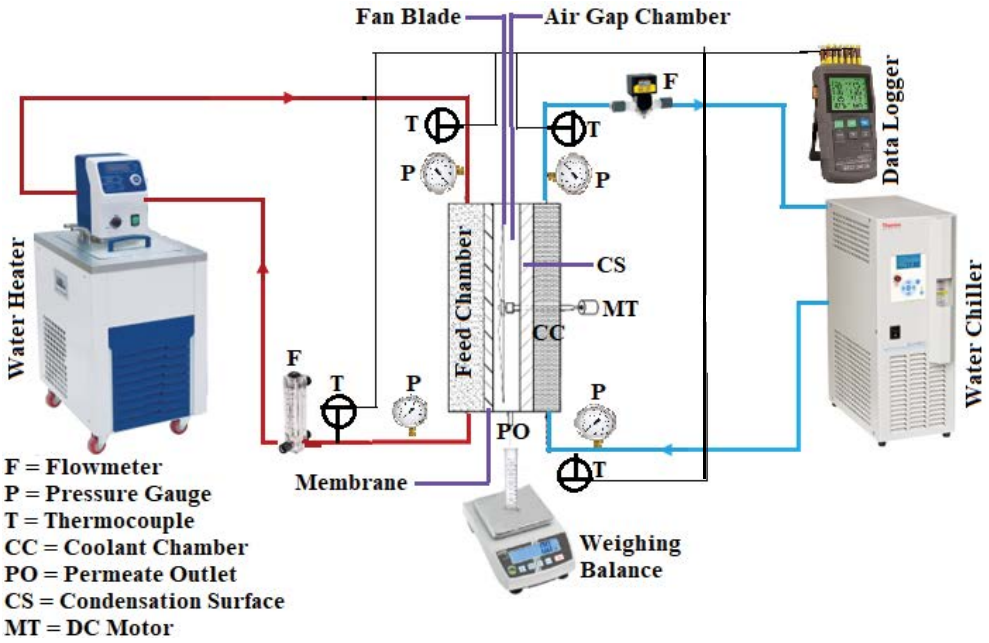

Fig. 3. Experimental test rig of the new AGMD system.

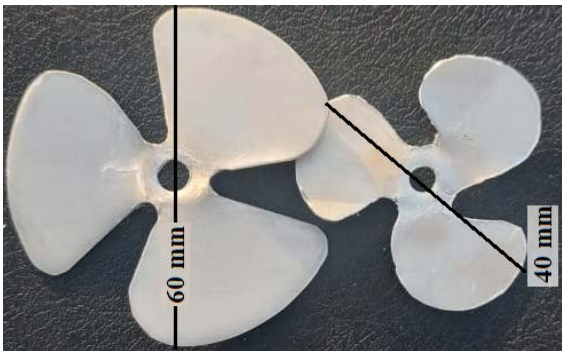

Fig. 4. Aluminum fan blade of different diameters.

where (kg/m²·h), (kg), (h), and (m²) indicate the vapor flux, weight of the collected permeate, duration of distillate collection, and the effective membrane area. The SR (%), (g/L), and (g/L) is the salt rejection efficiency, the feed concentration, and the permeate concentration.

The system specific thermal energy consumption, which represents the consumed thermal energy per unit volume of the produced distilled water, is represented by [14]:

$$\text{STEC} = \frac{\dot{Q}_{\text{feed}} + \dot{Q}_{\text{coolant}} + \dot{Q}_{\text{motor}}}{V_p}\left(\frac{\text{kWh}}{\text{m}^3}\right) \tag{3}$$

$$V_p = J_W \times A_{\text{em}} \times 10^{-3} \tag{4}$$

The DC motor consumed electric energy while providing rotational motion to the fan. This electrical energy is provided in the form of work, and it is converted to the equivalent thermal unit as used in Eq. (3). The fan equivalent thermal energy can be expressed as:

$$\dot{Q}_{\text{motor}} = \frac{\text{Motor power consumed}}{\text{Operating efficiency of panel}} \tag{5}$$

where V_p, J_w, A_{em}, $\dot{Q}_{\text{motor}}$, $\dot{Q}_{\text{feed}}$, and $\dot{Q}_{\text{coolant}}$ are the distillate volumetric flowrate (m³/h), water flux (kg/m²·h), membrane effective area (m²), fan equivalent thermal energy (kW), required heat input from water heater (kW), and thermal demand from water chiller (kW), respectively.

3. Results and discussion

The variation of vapor flux and specific thermal energy consumption with different fan diameters (40 and 60 mm) and without a fan at different feed temperatures is illustrated in Fig. 6a and b. At every feed temperature, the larger fan diameter recorded a higher flux and a lower STEC. A smaller fan diameter occupied a smaller gap area and displaced a smaller volume of water, resulting in a lower turbulence level and less heat and mass transfer enhancement. On the other hand, a larger fan diameter dispersed a larger volume of water in the gap, thereby setting all the water in the gap chamber to almost complete circulation and turbulence. This reduces the resistance to total heat and mass transfer within the gap chamber and improves the system flux and STEC. It is worth noting that higher heat and mass transfers encourage higher energy consumption. However, the enhancement in productivity due to the improvement in heat and mass transfer exceeded the deficit of higher energy consumption. Therefore, the system STEC slightly improves with the larger fan diameter. For instance, increasing the fan diameter from 40 to 60 mm improves the system STEC by a maximum of 2.7%, while the maximum improvement in the system flux is almost 14% at a feed temperature of 80°C. Also, the system performance in the absence of a fan (zero fan) is inferior to the case involving fan installation.

The presence of a rotating fan in the gap chamber enhances gap heat and mass transfer due to the improved turbulence level, reduction in the thermal boundary layer, and increase in suction on the permeate side of the membrane. For the feed temperature of 50°C–80°C, the mean improvement in the vapor flux and STEC of an 80 mm fan diameter over the zero fan is about 73% and 54%, respectively. It should also be noted that fan diameter has a stronger effect at higher feed water temperatures when compared to lower feed temperatures due to higher heat and mass transfer and an exponential rise in driving force at higher feed temperatures.

The effect of fan diameter on the system vapor flux and STEC at different fan revolutions is demonstrated in Fig. 7. It can be noticed that at different fan speeds ranging from 500 to 2,000 rpm, a larger fan diameter yielded better performance in terms of STEC and flux. However, electric power consumed by the motor is higher for the larger gap diameter by a mean percentage of almost 15% due to the larger

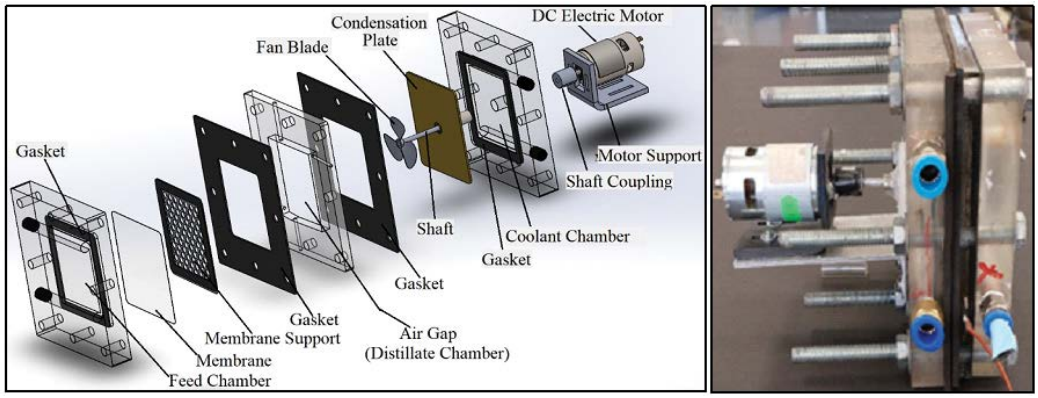

Fig. 5. An exploded view and a digital image of the new AGMD system.

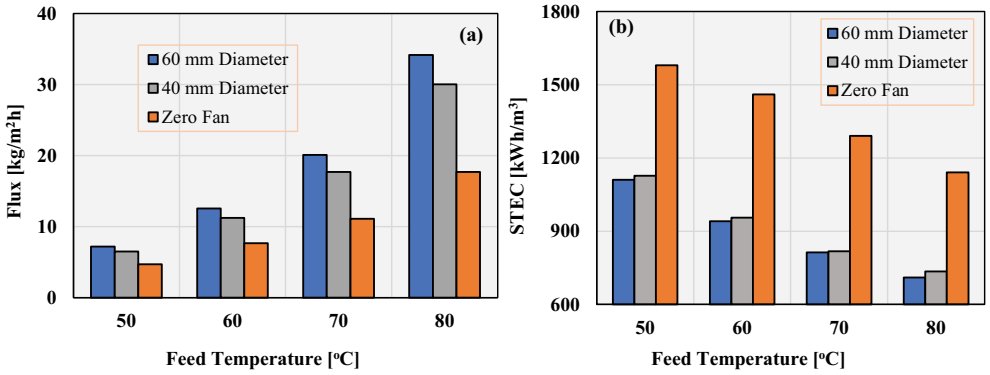

Fig. 6. Effect of fan diameter on flux and STEC at different feed stream temperatures. Test conditions: fan speed = 2,000 rpm, T_c = 20°C, m_c = 3 L/min, m_f = 3 L/min, 0.6 mm fan thickness.

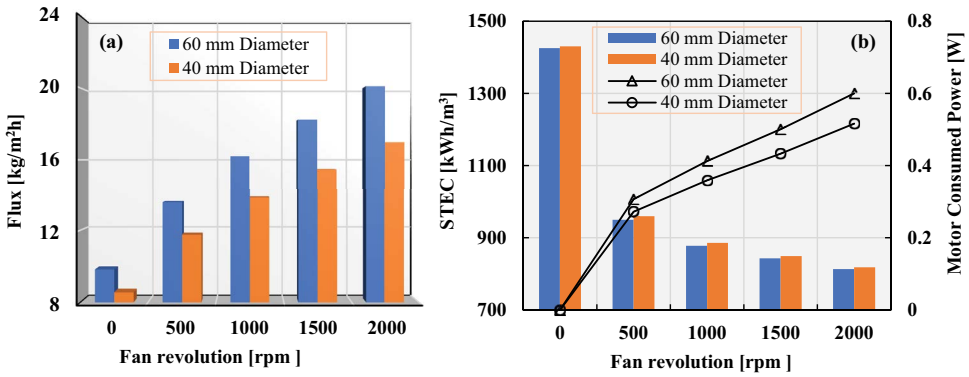

Fig. 7. Effect of fan diameter on flux and STEC at different fan revolution. Test conditions: T_f = 70°C, T_c = 20°C, m_c = 3 L/min, m_f = 3 L/min, 0.6 mm fan thickness.

weight associated with the larger gap. The larger the fan weight, the higher the electric power needed by the electric motor to drive the fan. With no fan in the gap, the system flux is low and the STEC is high. Whereas, with an installed fan inside the gap chamber, the system flux improves by 104.5% and the STEC decreases by 75.3% when operating the system at 2,000 rpm for the 60 mm fan diameter. The corresponding improvements for the 40 mm fan diameter are 98.6% and 74.8%, respectively. Also, increasing the fan revolution from 500–2,000 rpm increases the flux by about 48% and decreases the STEC by nearly 17% for the 60 mm fan diameter. The enhancement in system performance with the increasing fan revolution is predominantly due to the better mixing in the gap stream and the increase in the gap turbulent level. Higher fan revolutions also generate higher suction on the membrane and reduce the thermal boundary layer on the permeate side of the membrane.

Illustrated in Fig. 8 is the influence of fan blade thickness on the system flux and specific thermal energy consumption at different feed stream temperatures. Fan thicknesses of 0.6, 1.0, and 2.0 mm were considered in the study, and the findings indicate slightly better flux and STEC for thinner fan blade thicknesses. On average, over a feed temperature of 50°C–80°C, the system flux is raised by 5.23%, while the system STEC is dropped by just 0.89% in favor of 0.6 mm thickness and against 2.0 mm thickness. The marginal improvement recorded by the thinner fan blade against the thicker one may be attributed to the thinner fan blade's lesser resistance to heat transfer, which enhanced gap chamber heat and mass transfer characteristics.

The impact of fan blade thickness at various fan revolutions on the vapor flux and STEC is displayed in Fig. 9a and b. Over the fan speed range of 500 to 2,000 rpm, the 0.6 mm fan thickness attained a mean improvement of 3.61% and 1.02% in the system flux and STEC, respectively, over the 2.0 mm fan thickness. Hence, at every fan speed, thinner fan blades attained the highest flux and lowest STEC due to their lesser resistance to heat transfer when compared to thicker fan blades. It is worth mentioning that the influence of fan thickness is greater at higher fan revolutions because the highest improvement (6.84% for flux and 1.45 for STEC) is registered at 2,000 rpm, while the least improvement is attained at 500 rpm. A higher fan revolution is characterized by higher heat transfer activities through the thinner fan blade. Thus, the associated higher enhancement at higher fan revolution.

The price of freshwater production from the new AGMD design and the regular AGMD module without an installed fan is evaluated and represented in Fig. 10. The freshwater cost is calculated at feed stream temperature, feed stream flowrate, coolant stream temperature, coolant stream flowrate, air-gap width, feed concentration (TDS), fan blade thickness, fan diameter, and fan blade revolution of 70°C, 3 L/min, 20°C, 3 L/min, 11 mm gap, 35,000 mg/L,

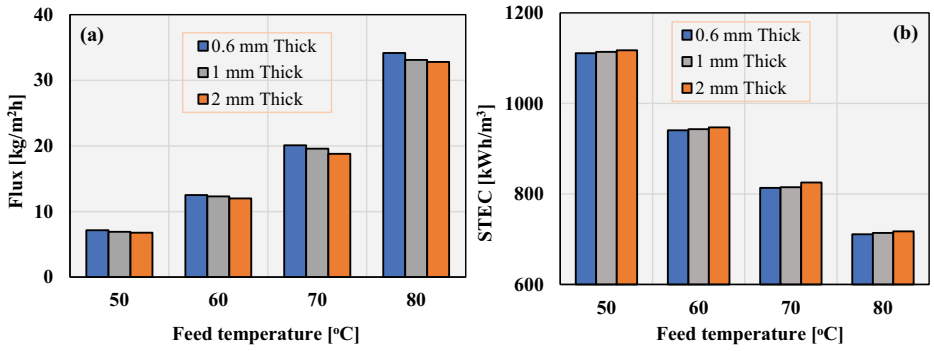

Fig. 8. Impact of fan thickness on flux and STEC at different feed stream temperatures. Test conditions: fan speed = 2,000 rpm, T_c = 20°C, m_c = 3 L/min, m_f = 3 L/min, 60 mm fan diameter.

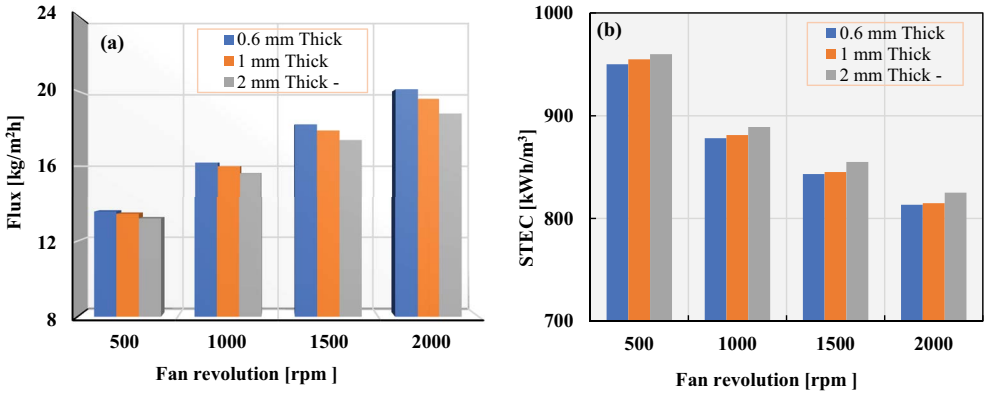

Fig. 9. Influence of fan thickness on flux and STEC at different fan revolution. Test conditions: T_f = 70°C, T_c = 20°C, m_c = 3 L/min, m_f = 3 L/min, 60 mm fan diameter.

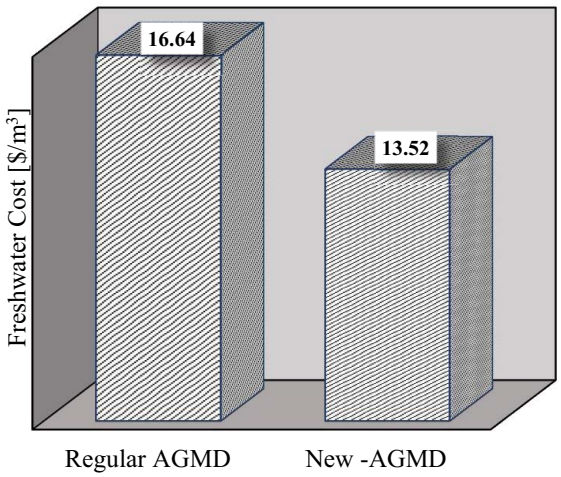

Fig. 10. Freshwater cost from the new and existing AGMD system.

0.6 mm, 60 mm, and 2,000 rpm, respectively, by using the cost model presented in [16,49]. The new AGMD module achieved an improved freshwater cost per unit volume over the regular/traditional AGMD module. The freshwater cost is reduced by over 23% by the new AGMD module, which may be attributed to the presence of a fan blade inside the gap chamber. The rotating fan enhances the heat and mass transfer characteristics of the new module, which improves system productivity significantly. The improved productivity is the major contributing factor to the lower freshwater cost of the new AGMD design.

It is worth mentioning that throughout the data collection, the salt rejection efficiency of the membrane and module was above 99.86%.

4. Conclusion

The performance of a new AGMD module in terms of vapor flux, specific thermal energy consumption, and freshwater production cost has been presented, analyzed, and compared to the conventional AGMD module. The system's performance is evaluated based on different fan blade thicknesses, fan diameters, fan revolutions, and feed stream temperatures. It can be concluded that fan speed significantly improves the performance of the new AGMD design compared to the conventional AGMD unit. Fan thickness recorded a marginal effect, and fan diameter registered some influence, while fan revolution exhibits the strongest impact on the system's performance. Operating the new AGMD unit at a fan revolution of 2,000 rpm, 70°C feed temperature, 20°C coolant temperature, 3 L/min feed flowrate, 3 L/min coolant flowrate, and 35,000 mg/L feed concentration increases the vapor flux by over 80%, decreases the system-specific thermal energy consumption (STEC) by over 58%, and reduces the price of freshwater by about 23%. Furthermore, elevating the feed water temperature from 50°C to 80°C improves the flux and STEC of the new AGMD design over the regular AGMD module, with a mean percentage enhancement of 72.76% and 54.2%, respectively. The new system can attain a maximum vapor flux and minimum STEC, of 34.16 kg/m^2·h and 710.72 kWh/m^3, respectively, as compared to the conventional units, which registered a peak flux and lowest STEC of 17.69 kg/m^2·h and 1,141.25 kWh/m^3, respectively. With further investigations and investments, the new AGMD design can provide cost-effective and affordable freshwater technology with the potential to compete with commercially available water desalination technology.

Acknowledgments

The work is supported by King Fahd University of Petroleum and Minerals (KFUPM) under the Interdisciplinary Research Center for Membranes and Water Security, Research Grant # INMW2203, and under the Deanship of Research Oversight and Coordination, Research Grant # SR191032.

References

[1] J. Li, L.-F. Ren, J. Shao, Y. Tu, Z. Ma, Y. Lin, Y. He, Fabrication of triple layer composite membrane and its application in membrane distillation (MD): effect of hydrophobic-hydrophilic membrane structure on MD performance, Sep. Purif. Technol., 234 (2020) 116087, doi: 10.1016/j.seppur.2019.116087.
[2] M. Khayet, J.I. Mengual, T. Matsuura, Porous hydrophobic/hydrophilic composite membranes: application in desalination using direct contact membrane distillation, J. Membr. Sci., 252 (2005) 101–113.
[3] S. Bonyadi, T.S. Chung, Flux enhancement in membrane distillation by fabrication of dual layer hydrophilic–hydrophobic hollow fiber membranes, J. Membr. Sci., 306 (2007) 134–146.
[4] J. Li, L.-F. Ren, H.S. Zhou, J. Yang, J. Shao, Y. He, Fabrication of superhydrophobic PDTS-ZnO-PVDF membrane and its anti-wetting analysis in direct contact membrane distillation (DCMD) applications, J. Membr. Sci., 620 (2021) 118924, doi: 10.1016/j.memsci.2020.118924.
[5] M. Qtaishat, D. Rana, T. Matsuura, M. Khayet, Effect of surface modifying macromolecules stoichiometric ratio on composite hydrophobic/hydrophilic membranes characteristics and performance in direct contact membrane distillation, AlChE J., 55 (2009) 3145–3151.
[6] B. Xie, G. Xu, Y. Jia, L. Gu, Q. Wang, N. Mushtaq, B. Cheng, Y. Hu, Engineering carbon nanotubes enhanced hydrophobic membranes with high performance in membrane distillation by spray coating, J. Membr. Sci., 625 (2021) 118978, doi: 10.1016/j.memsci.2020.118978.
[7] T. Pan, J. Liu, N. Deng, Z. Li, L. Wang, Z. Xia, J. Fan, Y. Liu, ZnO Nanowires@PVDF nanofiber membrane with superhydrophobicity for enhanced anti-wetting and anti-scaling properties in membrane distillation, J. Membr. Sci., 621 (2021) 118877, doi: 10.1016/j.memsci.2020.118877.
[8] C. Li, X. Li, X. Du, Y. Zhang, W. Wang, T. Tong, A.K. Kota, J. Lee, Elucidating the trade-off between membrane wetting resistance and water vapor flux in membrane distillation, Environ. Sci. Technol., 54 (2020) 10333–10341.
[9] S. Ding, T. Zhang, M. Wu, X. Wang, Photothermal dual-layer hydrophilic/hydrophobic composite nanofibrous membrane for efficient solar-driven membrane distillation, J. Membr. Sci., 680 (2023) 121740, doi: 10.1016/j.memsci.2023.121740.
[10] M. Darman, N. Niknafs, A. Jalali, Effect of wavy corrugations on the performance enhancement of direct contact membrane distillation modules: a numerical study, Chem. Eng. Process. Process Intensif., 190 (2023) 109421, doi: 10.1016/j.cep.2023.109421.
[11] Y. Wang, X. Liu, J. Ge, J. Li, Y. Jin, Distillation performance in a novel minichannel membrane distillation device, Chem. Eng. J., 462 (2023) 142335, doi: 10.1016/j.cej.2023.142335.
[12] D. Singh, L. Li, G. Obusckovic, J. Chau, K.K. Sirkar, Novel cylindrical cross-flow hollow fiber membrane module for direct

contact membrane distillation-based desalination, J. Membr. Sci., 545 (2018) 312–322.
[13] J.-H. Tsai, C. Quist-Jensen, A. Ali, Multipass hollow fiber membrane modules for membrane distillation, Desalination, 548 (2023) 116239, doi: 10.1016/j.desal.2022.116239.
[14] D. Lawal, M.A. Azeem, A. Khalifa, W. Falath, T. Baroud, M. Antar, Performance improvement of an air gap membrane distillation process with rotating fan, Appl. Therm. Eng., 204 (2022) 117964, doi: 10.1016/j.applthermaleng.2021.117964.
[15] S. Memon, B.-G. Im, H.-S. Lee, Y.-D. Kim, Comprehensive experimental and theoretical studies on material-gap and water-gap membrane distillation using composite membranes, J. Membr. Sci., 666 (2023) 121108, doi: 10.1016/j.memsci.2022.121108.
[16] S.M. Alawad, D.U. Lawal, A.E. Khalifa, I.H. Aljundi, M.A. Antar, T.N. Baroud, Analysis of water gap membrane distillation process with an internal gap circulation propeller, Desalination, 551 (2023) 116379, doi: 10.1016/j.desal.2023.116379.
[17] H.F. Juybari, H.B. Parmar, A.D. Alshubbar, K.L. Young, D.M. Warsinger, Porous condensers can double the efficiency of membrane distillation, Desalination, 545 (2023) 116129, doi: 10.1016/j.desal.2022.116129.
[18] D.U. Lawal, Performance enhancement of permeate gap membrane distillation system augmented with impeller, Sustainable Energy Technol. Assess., 54 (2022) 102792, doi: 10.1016/j.seta.2022.102792.
[19] C.-D. Ho, L. Chen, J.-Y. Lai, C.A. Ng, Theoretical and experimental studies of direct contact membrane distillation modules with inserting W-shaped carbon-fiber spacers, Desal. Water Treat., 71 (2017) 32–44.
[20] C. Wu, Y. Jia, H. Chen, X. Wang, Q. Gao, X. Lu, Study on air-bubbling strengthened membrane distillation process, Desal. Water Treat., 34 (2011) 2–5.
[21] C. Dong, Y. Huang, L. Zhang, Slug flow-enhanced vacuum membrane distillation for seawater desalination: flux improvement and anti-fouling effect, Sep. Purif. Technol., 320 (2023) 124178, doi: 10.1016/j.seppur.2023.124178.
[22] E.H. Cabrera Castillo, N. Thomas, O. Al-Ketan, R. Rowshan, R.K. Abu Al-Rub, L.D. Nghiem, S. Vigneswaran, H.A. Arafat, G. Naidu, 3D printed spacers for organic fouling mitigation in membrane distillation, J. Membr. Sci., 581 (2019) 331–343.
[23] G. Chen, X. Yang, R. Wang, A.G. Fane, Performance enhancement and scaling control with gas bubbling in direct contact membrane distillation, Desalination, 308 (2013) 47–55.
[24] M.C. Bhoumick, S. Roy, S. Mitra, Synergistic effect of air sparging in direct contact membrane distillation to control membrane fouling and enhancing flux, Sep. Purif. Technol., 272 (2021) 118681, doi: 10.1016/j.seppur.2021.118681.
[25] Y. Ye, S. Yu, L. Hou, B. Liu, Q. Xia, G. Liu, P. Li, Microbubble aeration enhances performance of vacuum membrane distillation desalination by alleviating membrane scaling, Water Res., 149 (2019) 588–595.
[26] C. Dong, Y. Huang, H. Lin, L. Zhang, Performance intensification and anti-fouling of the two-phase flow enhanced direct contact membrane distillation for seawater desalination, Desalination, 541 (2022) 116059, doi: 10.1016/j.desal.2022.116059.
[27] Y. Zhang, J. Sun, F. Guo, Performance enhancement for membrane distillation by introducing insoluble particle fillers in the feed, Desalination, 558 (2023) 116624, doi: 10.1016/j.desal.2023.116624.
[28] Y. Elhenawy, G.H. Moustafa, S.M.S. Abdel-Hamid, M. Bassyouni, M.M. Elsakka, Experimental investigation of two novel arrangements of air gap membrane distillation module with heat recovery, Energy Rep., 8 (2022) 8563–8573.
[29] S.-H. Kim, H.K. Lim, Improvement of membrane distillation performance through enhancement of the heat retaining capacity of the heat storage tank using phase change material, Desal. Water Treat., 97 (2017) 8–13.
[30] D.U. Lawal, M.A. Antar, K.G. Ismaila, A. Khalifa, S.M. Alawad, Hybrid multi-stage flash (MSF) and membrane distillation (MD) desalination system for energy saving and brine minimization, Desalination, 548 (2023) 116231, doi: 10.1016/j.desal.2022.116231.
[31] Y. Elhenawy, G.H. Moustafa, A.M. Attia, A.E. Mansi, T. Majozi, M. Bassyouni, Performance enhancement of a hybrid multi effect evaporation/membrane distillation system driven by solar energy for desalination, J. Environ. Chem. Eng., 10 (2022) 108855, doi: 10.1016/j.jece.2022.108855.
[32] R. Srivastava, A.K. Jaiswal, A. Jayakumar, J. Swaminathan, Internal feed preheating necessary for energy-efficient modular multi-effect membrane distillation, Desalination, 564 (2023) 116753, doi: 10.1016/j.desal.2023.116753.
[33] A. Najib, J. Orfi, E. Ali, A. Ajbar, M. Boumaaza, K. Alhumaizi, Performance analysis of cascaded membrane distillation arrangements for desalination of brackish water, Desal. Water Treat., 76 (2017) 19–29.
[34] T. Xiao, C. Liu, L. Liu, S. Wang, J. Tang, A nuclear driven hybrid sCO_2 power cycle/membrane distillation system for water-electricity cogeneration, Energy Convers. Manage., 271 (2022) 116329, doi: 10.1016/j.enconman.2022.116329.
[35] M. Ahmed, R.K. Alambi, G. Bhadrachari, S. Al-Muqahwi, J.P. Thomas, Design and optimization of a unique pilot scale forward osmosis integrated membrane distillation system for seawater desalination, J. Environ. Chem. Eng., 11 (2023) 109949, doi: 10.1016/j.jece.2023.109949.
[36] Y. Elhenawy, K. Fouad, M. Bassyouni, T. Majozi, Design and performance a novel hybrid membrane distillation/humidification–dehumidification system, Energy Convers. Manage., 286 (2023) 117039, doi: 10.1016/j.enconman.2023.117039.
[37] Y. Elhenawy, M. Bassyouni, K. Fouad, A.M. Sandid, M.A. El-Rady Abu-Zeid, T. Majozi, Experimental and numerical simulation of solar membrane distillation and humidification – dehumidification water desalination system, Renewable Energy, 215 (2023) 118915, doi: 10.1016/j.renene.2023.118915.
[38] T. Arthur, G.J. Millar, E. Sauret, J. Love, Renewable hydrogen production using non-potable water: thermal integration of membrane distillation and water electrolysis stack, Appl. Energy, 333 (2023) 120581, doi: 10.1016/j.apenergy.2022.120581.
[39] N.A.A. Qasem, D.U. Lawal, I.H. Aljundi, A.M. Abdallah, H. Panchal, Novel integration of a parallel-multistage direct contact membrane distillation plant with a double-effect absorption refrigeration system, Appl. Energy, 323 (2022) 119572, doi: 10.1016/j.apenergy.2022.119572.
[40] N.T.U. Kumar, A. Martin, Techno-economic optimization of solar thermal integrated membrane distillation for cogeneration of heat and pure water, Desal. Water Treat., 98 (2017) 16–30.
[41] J. Orfi, A. Najib, E. Ali, A. Ajbar, M. AlMatrafi, M. Boumaaza, K. Alhumaizi, Membrane distillation and reverse osmosis-based desalination driven by geothermal energy sources, Desal. Water Treat., 76 (2017) 40–52.
[42] D.U. Lawal, A.E. Khalifa, Experimental investigation of an air gap membrane distillation unit with double-sided cooling channel, Desal. Water Treat., 57 (2016) 11066–11080.
[43] A.E. Khalifa, Flux enhanced water gap membrane distillation process-circulation of gap water, Sep. Purif. Technol., 231 (2020) 115938, doi: 10.1016/j.seppur.2019.115938.
[44] J. Swaminathan, H.W. Chung, D.M. Warsinger, F.A. AlMarzooqi, H.A. Arafat, J.H. Lienhard V, Energy efficiency of permeate gap and novel conductive gap membrane distillation, J. Membr. Sci., 502 (2016) 171–178.
[45] L. Francis, N. Ghaffour, A.A. Alsaadi, G.L. Amy, Material gap membrane distillation: a new design for water vapor flux enhancement, J. Membr. Sci., 448 (2013) 240–247.
[46] L.-H. Cheng, Y.-H. Lin, J. Chen, Enhanced air gap membrane desalination by novel finned tubular membrane modules, J. Membr. Sci., 378 (2011) 398–406.
[47] V.T. Shahu, S.B. Thombre, Experimental analysis of a novel helical air gap membrane distillation system, Water Supply, 21 (2021) 1450–1463.
[48] R. Aryapratama, H. Koo, S. Jeong, S. Lee, Performance evaluation of hollow fiber air gap membrane distillation module with multiple cooling channels, Desalination, 385 (2016) 58–68.
[49] S. Al-Obaidani, E. Curcio, F. Macedonio, G. Di Profio, H. Al-Hinai, E. Drioli, Potential of membrane distillation in seawater desalination: thermal efficiency, sensitivity study and cost estimation, J. Membr. Sci., 323 (2008) 85–98.